






Sputtered highly effective iridium catalysts: a new approach for green satellite propulsion

Manfred Stollenwerk^{1,*} , Tobias Schäfer¹, Johannes Stadtmüller¹, Thorsten Döhring¹ ,
Dominic Freudenmann² , and Nicole Röcke²

¹TH Aschaffenburg – University of Applied Sciences, Würzburger Straße 45, 63743 Aschaffenburg, DE, Germany

²Institute of Space Propulsion – Chemical Propellant Technology, Department, German Aerospace Center (DLR), Im Langen Grund, 74239 Hardthausen, DE, Germany

Received: 2 December 2020

Accepted: 4 February 2021

Published online:

1 March 2021

© The Author(s) 2021

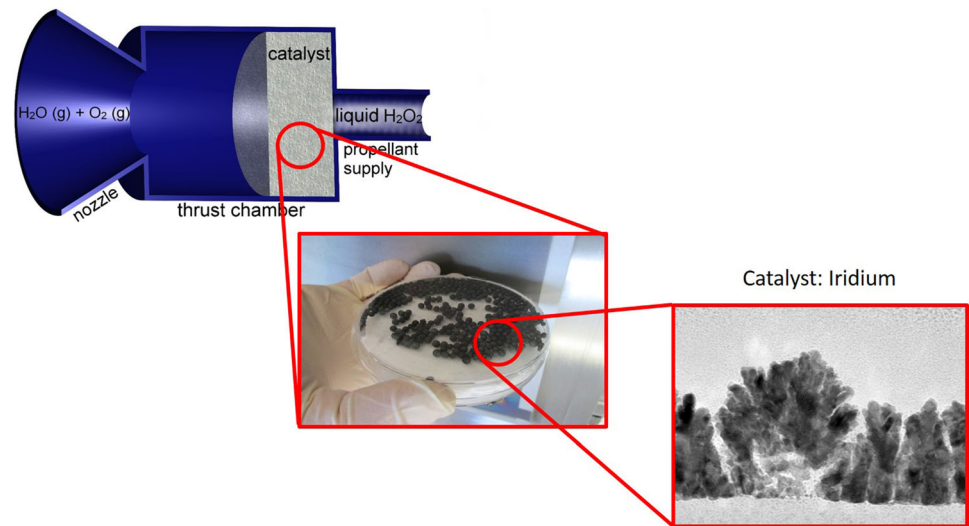
ABSTRACT

This work demonstrated the large potential of sputtered iridium metal for catalytic reactions shown by the example of decomposition of hydrogen peroxide (H_2O_2) for space propulsion systems. For this purpose, iridium was coated onto Al_2O_3 pellets by a sputter process under varied process parameters. Depending on previously selected parameters, the obtained metal-loaded pellets offer closed- and/or open-shell structures. Catalytic productivity of these first-generation iridium-sputtered catalysts was estimated in laboratory experiments and compared to platinum-loaded pellets. Under optimized sputter-process conditions, the reactivity is significantly improved compared to the platinum-impregnated pellets. The better catalytic productivity can be explained by the increased active surface area of the iridium layers on the pellets. The surface morphology and the microstructure of the iridium coating can be actively controlled by the sputter pressure. The results are in accordance with the sputtering process pressure tendency described by the Thornton Structure–Zone Model.

Handling Editor: Maude Jimenez.

Address correspondence to E-mail: manfred.stollenwerk@th-ab.de

GRAPHICAL ABSTRACT



Introduction

Application of heterogeneous catalysis of green propellants in space technology

The need for propellants with reduced toxicity and aggressiveness combined with lower required safety precautions during transportation, storage and handling is a main driver in today's propellant technology: Efforts are being made in the EU which will probably restrict the use of hydrazines (e.g. N_2H_4) and dinitrogen tetroxide (NTO) in propulsion systems for space vehicles in the near future [1]. These toxic substances are still widely used in mono- or bipropellant propulsion systems and have been flight-proven over decades [2]. A green propellant substitute for hydrazine in monopropellant-based propulsion systems is rocket-grade hydrogen peroxide [3]. Although hydrogen peroxide has been used since the early days of rocketry and aviation, industrial production has made progress and opened the market to commercially available hydrogen peroxide of high purity and in sufficient quantities [4].

Noble metals as active catalyst in space applications

Hydrogen peroxide decomposes in an exothermic reaction to water steam and oxygen gas by help of catalytically active materials. Upon contact of the catalyst with aqueous solutions of hydrogen peroxide, the decomposition reaction will start and will be proportionately accelerated by rising reaction temperatures. Therefore, high-concentration solutions of hydrogen peroxide can be used as a mono- or bipropellant in propulsion systems [5]. Typical materials that are used as active catalyst phase are members of the platinum group (platinum, iridium), which are mainly chemically dispersed on ceramic catalyst beads (e.g., aluminum oxides) [6]. Besides the efficiency of combustion of those catalysts at even ambient temperatures, most of the state-of-the-art catalysts are used in a pre-heated mode. Noble metals of the platinum group have as common features suitable resistance to oxidation, sufficient thermal stability, and a high affinity toward catalytic peroxide decomposition [7]. These features make them valuable key players in catalytic-driven monopropellant propulsion systems, working in pulse trains or in continuous-firing mode [8]. Compared to bipropellant combinations and hydrazines as

monopropellant, the calculated adiabatic decomposition temperature for highly concentrated hydrogen peroxide is reduced (~ 950 °C) and will therefore limit the risk of high-rate metal oxidation or ablation [9]. In the following experimental concepts and considerations, this value is also used as benchmark.

Although manganese oxide catalysts have been used in the early days of rocket propulsion for the decomposition of hydrogen peroxide [10], we focus within this paper on noble metals as more “modern” catalysts, especially on iridium and platinum.

Sputtered films as catalyst

Besides the above-mentioned methods to use platinum or iridium, many applications in the form of thin films for catalytic applications are known [11–13]. The main reason for this usage is the cost-saving compared to bulk material. One method to deposit thin catalytic films is a physical method such as PVD (physical vapor deposition, sputtering) [11, 14–16]. However, the sputtering method to deposit platinum or iridium for catalytic applications is currently rarely used; most of the publications describe the usage of sputtered platinum and/or iridium as catalysts in proton exchange membrane fuel cells. As early as 1979, Beni et al. [17] demonstrated that electrocatalysts for oxygen evolution electrodes can be produced by sputtered Ir–O films. Mukerjee et al. [18] studied in 1993 the effect of sputtered iridium on the kinetics of oxygen reduction. Atanasoski et al. [19] compared different rare earth materials sputtered on Pt-coated nanostructured thin films. Alvisi et al. [20] could achieve significantly higher activity for MeOH oxidation with sputter-deposited platinum films compared to conventional catalysts. The goal of Hirano et al. [21] was to minimize the Pt-loading in catalysts cells. Ganske et al. [22] and Tapalov [23] investigated the catalytic activity of different Ir/Pt ratios. In two different publications, Slavcheva et al. described the influence of sputter parameters on the surface structure and on the catalytic effects of sputtered platinum [24] and iridium [25]. A systematic variation of process parameters such as power, pressure, and target-to-substrate distance is described in publications by Wessling et al. [26–28], including a simulation of the sputter process in one publication [29].

Most of the current publications concerning sputtered iridium catalysts are dealing with the usage of

these layers for Proton Exchange Membranes (PEM), water splitting, Oxygen Evolution Reaction (OER) and Hydrogen Evolution Reactions (HER) [30].

In this study, we experimentally investigated sputtered iridium films for the decomposition of aqueous hydrogen peroxide solutions for later application in propulsion systems. The porosity of the deposited iridium layers should be tuneable by adjusting the process gas pressure during the sputtering process. Transmission electron microscopy (TEM), scanning electron microscopy (SEM) and energy-dispersive X-ray spectroscopy (EDX) measurements were performed to examine morphology, microstructure, thickness and elemental composition of the obtained iridium layers. Following the sputtering process, an experimental decomposition test and thermal stability measurements of the prepared iridium pellets are of high interest. Oxygen-rich environments and increasing temperatures that are achievable in a model combustor chamber are of a challenging in nature concerning material oxidation or ablative effects.

First simulations of these environmental conditions can roughly be performed in thermogravimetric (TG) and dynamic differential calorimetry (DSC) apparatus under oxygen-rich gas flow and high temperatures. Within this experimental approach, worst-case conditions (1000 °C, oxygen-rich atmosphere) were chosen. Experimental outcomes give a first impression at material stability and thermal properties of the produced pellets.

Experimental

Preparation of pellets and sputtering process

The iridium thin films were prepared by radio frequency (RF) magnetron sputtering using equipment from Aurion Anlagentechnik with a high-purity (99.9%) iridium target. The distance between the target and the substrate was set to 120 mm, and the inclination angle between the target and the normal to the substrate was set to 40° and a sputtering power of 300 W was used. As process gas, high purity argon (99.999%) was used. The process pressure during coating was actively controlled by a throttle valve, in front of the pump combination of rotary pump and turbo molecular pump, independently from the

argon flow. After loading the chamber with the substrates (Al_2O_3 pellets or flat glasses), the system was pumped down to $5.0 \cdot 10^{-5}$ hPa to remove the remaining gases. The sputter processes started after the argon gas flow was set to 50 sccm and the chosen process pressure was stabilized. Two different batches (named A and B in the following text) were coated using different process pressures ($p_A = 3 \cdot 10^{-2}$ hPa and $p_B = 5.0 \cdot 10^{-3}$ hPa). To achieve better uniformity of the films, the substrates were rotated at 8 rpm during sputtering. Neither heating nor cooling was applied to the substrates. The pellets were placed on a structured substrate holder (metal lattice), as shown in Fig. 1.

The coatings were performed in two steps to ensure a coating of the complete pellet surface. After the first step, the coating chamber was flooded with air, opened, and the pellets were turned upside-down by hand. Afterward, the second process step was started, again with pumping down and using the same process conditions. To estimate the coating thickness, some flat glass substrates were coated additionally, and on these glass substrates the film thickness was measured using a Dektak XT profilometer from Bruker, equipped with a stylus of radius $12.5 \mu\text{m}$. The reproducibility of the layer thickness on flat substrates is (for identical sputter process conditions) better than $\pm 2\%$. However, the thickness distribution on the Al_2O_3 pellets is strongly depending on the individual surface morphology of the fissured pellets. Additional uncertainties of the layer thickness occur due to the described turning of

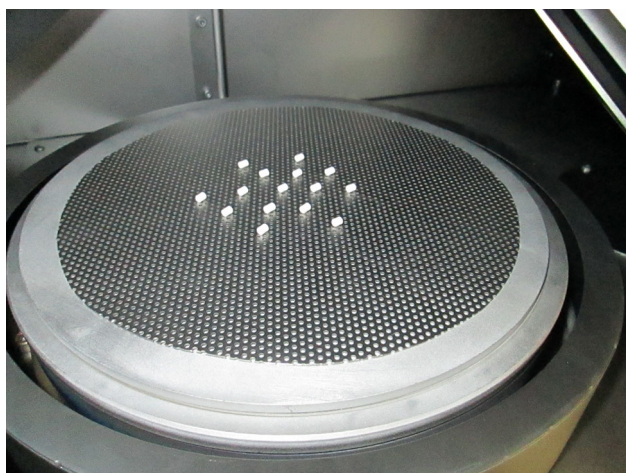


Figure 1 Sputter chamber loaded with the Al_2O_3 pellets. The sputter cathode can be seen at the right top corner.

the pellets to ensure the complete coating of the pellets. Both batches are treated in the same way.

To achieve comparability (i.e. surface morphology, dimensions) in the decomposition experiments, iridium was coated on the same type of pellets (diameter ca. 2 mm, length 5 mm) which were used as reference platinum pellets. For this purpose, industrially manufactured Al_2O_3 pellets loaded with 1% of platinum were used (formerly Degussa, F 26 P). Blank pellets for the sputtering process were obtained the following way: Pt-loaded pellets from Degussa were treated twice with boiling aqua regia and washed with purified water to remove all platinum before sputtering. The success of complete removal of platinum was proven with EDX analysis at different positions on the pellets. This procedure removes loose Al_2O_3 particles in/on the pellets, too.

Analytical methods

SEM and TEM analysis

Cross-sections of iridium films were investigated using an FEI TECNAI T20 transmission electron microscope (TEM) equipped with a LaB 6 filament. An electron-transparent lamella of the iridium coated sample (flat glass and pellet) perpendicular to the film plane was prepared by focused ion beam (FIB) using a Helios NanoLab 600i, followed by argon ion etching with a PIPS II polishing system. The surfaces of the iridium-coated pellets were analyzed using a Phenom ProX Desktop Scanning Electron Microscope including energy-dispersive X-ray spectroscopy (EDX) to determine the elemental composition.

Thermal analysis

Thermogravimetric (TG) and dynamic differential calorimetry (DSC) measurements were performed with a NETZSCH Jupiter STA 449F in oxygen-rich gas flow (50 mL min^{-1}), in Al_2O_3 crucibles. In a typical experiment, Ir-loaded pellets were heated at a rate of 10 K/min to the final temperature. The measuring curves were corrected by subtracting a previous measured buoyancy curve which eliminated lifting effects caused by the gas flow at raising temperatures. Evolved gaseous species were detected by Fourier-transform infrared spectroscopy (FTIR spectroscopy) with a coupled BRUKER ALPHA FTIR spectrometer.

Catalytic effects

Perhydrol (solution of 30 wt % H_2O_2 in water) was used in the experiments as model liquid in a gas collecting apparatus built in our laboratory. Concentration of the aqueous H_2O_2 solution was validated before initialization of the test sequence by density measurement. The reaction chamber was a double-walled glass cylinder with water as thermostating liquid occupying the annular space between the double walls. The water constantly circulated through a thermostat at ambient conditions (22 °C). A thermometer displayed the temperature of the peroxide solution. The apparatus was sealed by a glass flange, providing gas-tight conditions. Collection and readout of the volume of the evolved gas were done visually by a glass syringe (100 mL, Fortuna Optima) where the syringe barrel and plunger were sealed with PTFE (see Fig. 2).

The whole apparatus was washed three times with water and ethanol separately to remove any traces of impurities and flushed to dryness with nitrogen afterward. Prior to the start of each experiment, gas

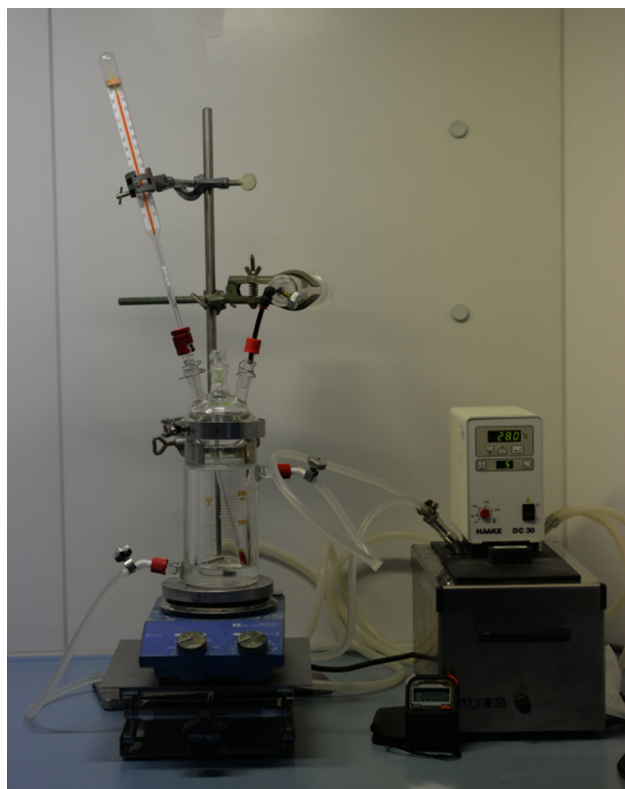


Figure 2 Gas collecting apparatus with installed thermostat and measuring equipment.

tightness of the apparatus was proven by applying a slight positive pressure of nitrogen gas and checked for potential gas emission using leak detection spray (OKS 2801). Experiments were performed successively with 10 pellets of each batch and Pt- reference material in 60 mL of freshly bottled perhydrol. All pellet charges were used sequentially according to Table 1 and tested within one day. Each setup was cleaned, dried and checked before a new pellet charge was investigated.

The liquid was then allowed to equilibrate to thermostat temperature in the darkened reaction vessel. Time was recorded at first contact of pellets with the liquid.

Results

Experimental investigations of the catalytic productivity of Ir-coated pellets

Results of the experimental investigations of the catalytic productivity of the two different processed pellet batches compared to Pt-loaded samples are summarized in Table 1. In general, the amount of released oxygen gas was measured at three different points in time (excluding the starting point at 0 s), and perhydrol temperature was recorded at the end of each measuring procedure. Measurement errors are principally based on reading errors and scaling effects of the syringe volume during data acquisition. Here, measured values of higher volumes are less faulty than those obtained in lower regimes. It is therefore assumed that the obtained values show an inaccuracy of approximately less than ± 1 mL.

During the experiment, photographs of the reaction during perhydrol decomposition were taken. In Fig. 3, an example image of the ongoing reaction (left) with used pellets (right) are presented.

For better comparison, Fig. 4 shows closeup photographs of nine pellets before (Fig. 4a) and after hydrogen peroxide treatment (Fig. 4b). Compared to the freshly prepared material, no significant optical changes in the overall appearance of the pellets are detectable. Moreover, no solid remnants were found at the bottom of the glass vessel, indicating ongoing ablation effects during reaction progress under the given conditions.

In Fig. 5, obtained data points are plotted in a turnover vs time curve and displayed by a

Table 1 Released amount of oxygen gas for measurements with 10 pellets each

Batch	Sputtering pressure [hPa]	V(O ₂)	V(O ₂)	V(O ₂)	V(O ₂)	End temp. of the liquid [°C]
		0 s [mL]	30 s [mL]	60 s [mL]	300 s [mL]	
A, 0.5 wt %	$3 \cdot 10^{-2}$	0	6	12	100	28
B, 0.5 wt %	$5 \cdot 10^{-3}$	0	1.5	3	32	26
Pt pellet, 1 wt %	NA	0	1	4	33	27

Figure 3 Photographs of the reaction vessel with ongoing reaction (a) and freshly prepared Iridium coated pellets (b).

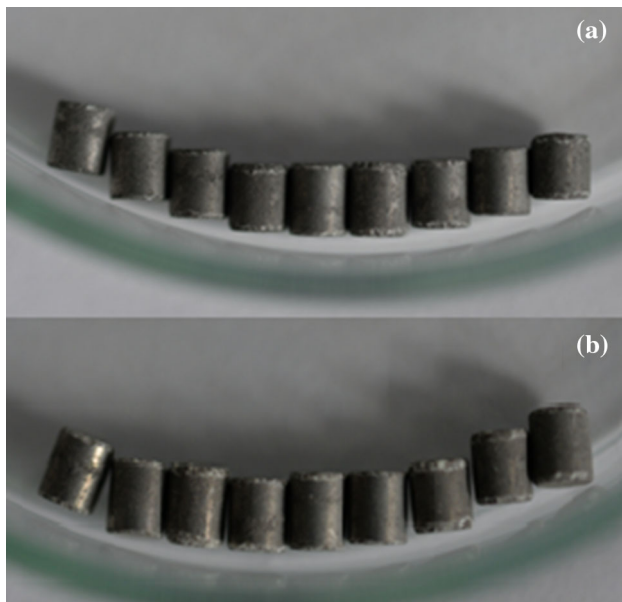
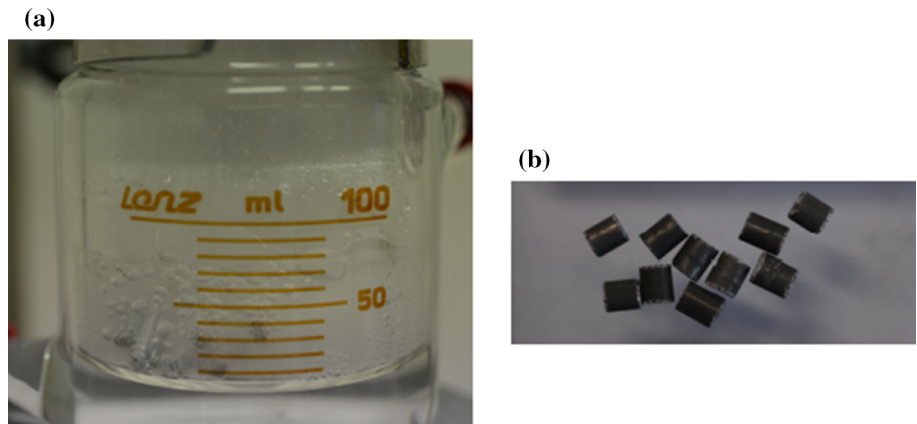


Figure 4 Photographs of some Ir-pellets before (a) and after reaction (b).

logarithmic curve. Under the given experimental conditions, gas release capability of the platinum pellets was equal to that of pellets of batch B. The curve that reveals much higher gas volumes was obtained with the batch A pellets. Increasing liquid temperature and gas release indicates a spontaneous, self-accelerating exothermic reaction.

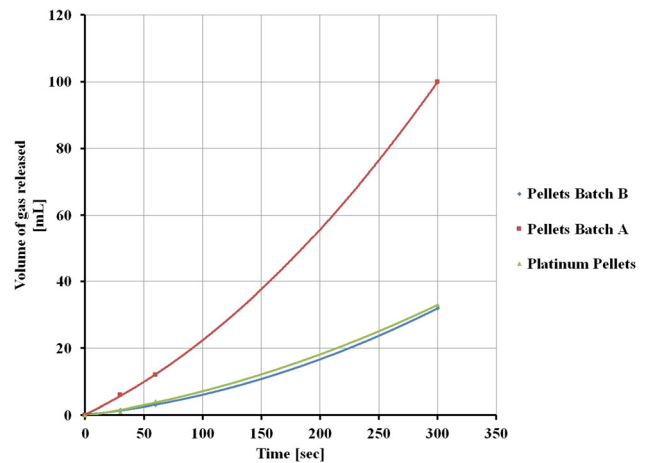


Figure 5 Plotted logarithmic curve of the experimentally obtained data points.

This finding is in accordance with the assumption of an increased active metal surface area on the pellets, originating from different process pressures during sputtering. On glass substrates, the coating time of 1080 s leads to nearly equal layer thicknesses of approximately 190 ± 10 nm at both used sputtering pressures. The corresponding relative mass of the iridium layer has been calculated as about 0.5 wt % for a typical cylindrical pellet, considering an iridium density of 20 g/cm^3 . Therefore, an effect of the layer thickness for the observed increase of the catalytic

efficiency can be ruled out. The cause lies rather in some aspect of the iridium layer that differs as a function of the different used process pressures.

Thermal analysis of sputtered Ir-coated pellets under oxygen-rich conditions

In Fig. 6, thermogravimetric (TG, black line) and dynamic differential calorimetry (DSC) curves (dotted line) of uncoated and Ir-sputtered Al_2O_3 pellets are presented (from top to bottom). While the TG/DSC curves of an uncoated pellet remain unremarkable, curves of the coated samples reveal significant changes.

In general, the recorded TG curve of an Ir-sputtered sample reveals a stepwise mass decrease during heating to 1000 °C final temperature. In sum, three weakly defined steps are detectable without reaching a final plateau at even higher temperatures (< 1000 °C). It is therefore assumed that, at first stage (~ 100 °C), mass loss is dominated by the evaporation of gases or adsorbed water which is near to the surface of the pellet.

This assumption is also validated by recorded FTIR spectra of the evolved gas species. Here, only carbon

dioxide and gaseous water are detectable as gaseous species. The medium temperature range at roughly 100 °C to 500 °C is dominated by a weight loss of yet unknown origin.

At temperature regimes above 500 °C, the observed mass loss could be explainable by slow metal oxidation into iridium(IV) oxide followed by evaporation. The observable exothermic DSC peak may originate from this oxidation process. Moreover, it is known in the literature that the iridium(III) oxide phase is maintained by chemical vapor transport of iridium(IV) oxide in oxygen-rich atmospheres at temperatures above 1000 °C [31]. A similar process could take place here. This assumption is underlined by the fact that discoloration of the pellet after the heating process is observable. Moreover, the nano-sized nature of the iridium crystallites could lead to changes of material properties. Similar effects on material conditions (e.g., change of boiling or melting point) that are caused by nanosized materials are extensively described in the scientific literature [32, 33]. In further experiments, an Ir-coated pellet was exposed to harsh conditions in a muffle furnace: For this purpose, the sample was heated to 1000 °C in air and then maintained at this temperature for 1 h. Results are presented in Fig. 7, clearly showing the complete removal of the deposited iridium layer.

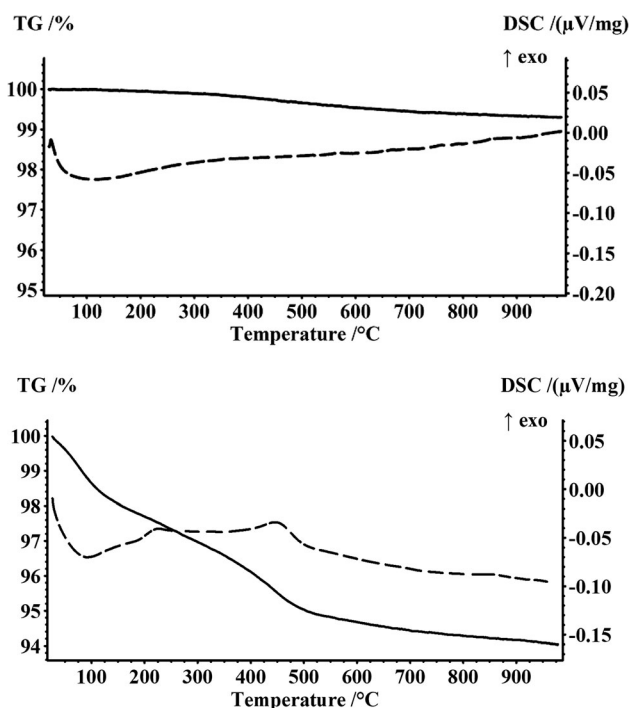


Figure 6 Thermogravimetric (TG) and dynamic differential calorimetry (DSC) curves of an uncoated (above) and Ir-coated pellet (bottom) under oxygen-rich conditions.

Discussion

The fact that the catalytic efficiency of sputtered iridium layers depends on the sputter parameters, such as pressure, substrate temperature, composition, bias voltage, is already known. For example, Ganske et al. [22] and Topalov et al. [23] described the catalytic effect of sputtered platinum–iridium layers for hydrogen fuel cells as dependent on the Pt–Ir ratio and the sputtering power. Wessling [28, 29] evaluated and simulated the electrochemical performance of sputtered iridium as dependent on the sputter pressure. The very strong dependence of the catalytic efficiency on the working gas sputter pressure seen in our study can be explained by the different layer structures for different sputter pressures: Fig. 8 shows transmission electron microscopy (TEM) cross-sections of sputtered iridium layers for the two used different sputter pressures. The iridium layers for these TEM investigations had been deposited on glass substrates with identical process parameters as

Figure 7 Photographs of an Ir pellet before (a) and after heat process (bright) (b).

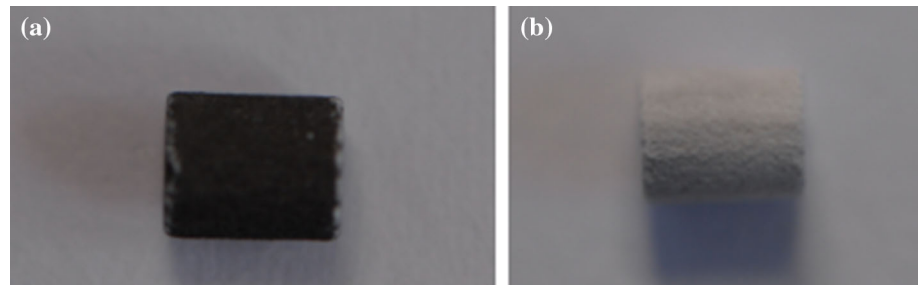
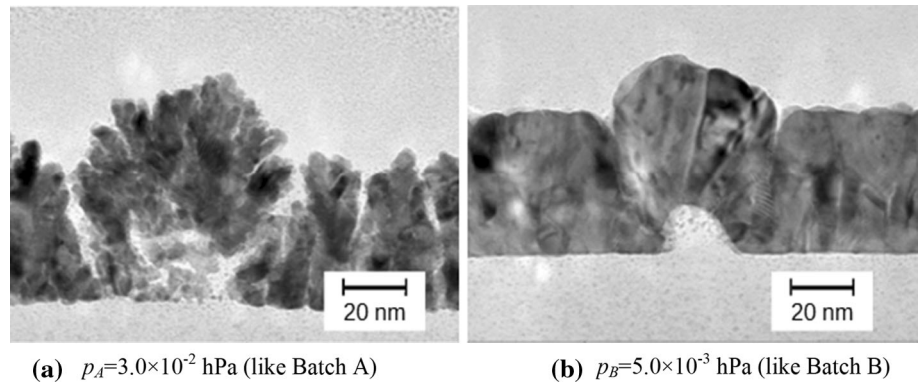


Figure 8 Transmission electron microscopy (TEM) cross-sections of sputtered iridium layers on glass substrates for different sputter pressures.



for the Al_2O_3 pellets (except coating time), because the sample preparation for the TEM images with glass substrates is much easier and the results are more concise compared to TEM images of layers deposited on the brittle Al_2O_3 pellets, as described later.

At low argon pressures ($p_B = 5 \cdot 10^{-3}$ hPa; Fig. 8b), the iridium layers had grown in columnar fashion, and clear grain boundaries can be identified. The layer surface is very smooth. Small irregularities of the substrate are covered complete by the Iridium layer.

With increasing argon pressure ($p_A = 3 \cdot 10^{-2}$ hPa; Fig. 8a), the layer structure appears fissured. Columns are separated by voids; a cauliflower-like structure appears. Also, the iridium crystals are smaller. Diffraction pattern reveals that the crystals have all different crystallographic orientations [34]. Defects of the glass surface lead to an additionally increased disoriented and rugged layer structure, with a significantly increased iridium surface area as shown in Fig. 8a, too.

This influence of the process pressures on the layer morphology is mainly caused by the interaction between argon and iridium atoms. A higher sputter pressure leads to an increase of the collisions of the iridium atoms with the argon process gas atoms before reaching the substrate. This results in lower

incident energies and a loss of the directionality of the iridium atoms arriving at the substrate or coating layer surface. At lower sputter pressures, the iridium atoms reaching the substrate or layer surface have a higher kinetic energy, which leads to higher surface mobility of the atoms [28, 29, 34]. Therefore, these atoms build more dense layers with an even surface area, following the concept described by the Thornton-Structure-Zone Model [35, 36].

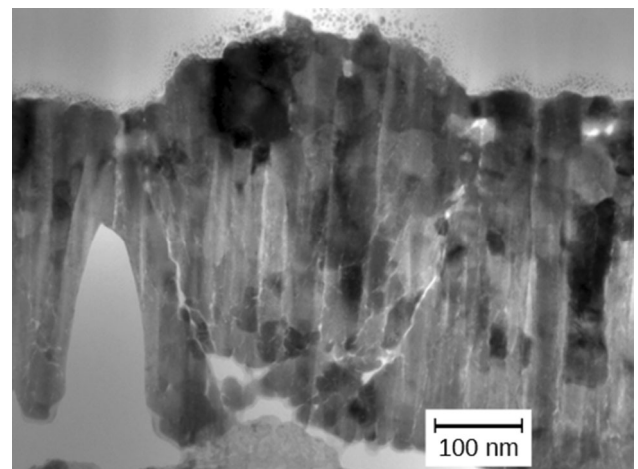


Figure 9 TEM analysis of iridium layers (sputtered with a pressure of $p_A = 3 \cdot 10^{-2}$ hPa) on Al_2O_3 pellets. Because of the fragile Al_2O_3 substrate, the TEM specimen for this picture is thicker than the glass samples in Fig. 5.

The described TEM analysis of iridium layers sputtered on glass is confirmed by similar analysis of iridium layers on Al_2O_3 pellets, as shown in Fig. 9.

The sputtered layers show the same growth mechanism as on a glass substrate. In addition, the structure of the Al_2O_3 increases the surface roughness and surface area of the iridium coating. Figure 10 shows a scanning electron microscope (SEM) picture of an uncoated Al_2O_3 pellet at low resolution.

The Al_2O_3 pellets have intentionally a very rough and inhomogeneous structure. Some areas are rougher than other areas. Therefore each pellet is different. However, this diversity should have no effect on the observed increased catalytic effect because the same structured pellets (loaded with platinum) had been used for the reference measurements. Additionally, an averaging takes place over the 10 pellets used in each batch.

The rugged structure of the pellet will additionally increase the disturbance of the iridium growth and may lead to an even larger iridium surface area than for coatings on glass surfaces, which may even increase the catalytic reactivity.

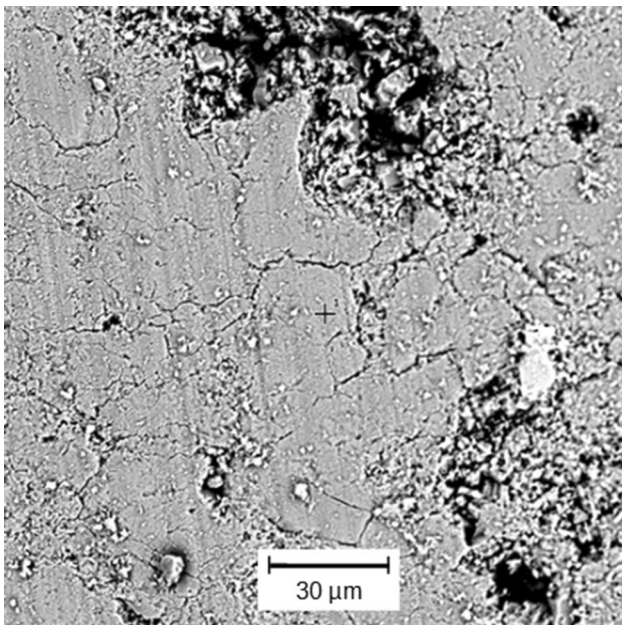


Figure 10 Scanning electron microscopy (SEM) picture of an uncoated Al_2O_3 pellet surface (after removal of the platinum in aqua regia and washed with purified water as described in chapter 2.1), at low resolution.

Conclusion and outline

Al_2O_3 pellets were coated with iridium by a sputtering process. It was shown that the surface morphology is highly tuneable by variation of process parameters, leading to more porous and/or more closed metal structures. Surface morphology was characterized by SEM and TEM images whereas TG and DSC measurements were performed to study the thermal properties of the materials. In first laboratory experiments, Ir-coated pellets showed a high tendency toward catalytic decomposition of aqueous hydrogen peroxide solutions. Here, a clear correlation between gas release and sputtering parameters is recognizable. As a reference, platinum-loaded pellets of the same substrate type were used, although the mass of platinum was about twice the mass of iridium for these pellets. Experiments verified that sputtered Ir-coated pellets with an open porous structure have superior catalytic productivity among the examined samples. TG and DSC analysis revealed that the sputtered iridium metal tends to evaporate at dry and harsh conditions after a period of time.

Therefore, similar effects are expected in rocket motors but, depending on the experimental setup and conditions, much less marked. The results obtained so far show the highly beneficial approach of new catalyst design using sputtering technology also for other catalytic applications. Within this new approach, hot gas tests with rocket-grade hydrogen peroxide (> 87%wt. H_2O_2) and extended lab-tests (e.g. lifetime of the coated Ir-pellets) are currently in preparation.

Acknowledgements

The authors are grateful to the M11 team of the Satellite and Orbital Propulsion Department at the Institute of Space Propulsion. We also thank Stefan Belle (Aschaffenburg University) and Christine Damm (IWF Dresden) for their support.

Funding

Open Access funding enabled and organized by Projekt DEAL.

Compliance with ethical standards

Conflict of interest The authors declare that they have no known competing financial interests or personal relationships that could have appeared to influence the work reported in this paper. The authors declare, that conflicts of interest do not exist.

Open Access This article is licensed under a Creative Commons Attribution 4.0 International License, which permits use, sharing, adaptation, distribution and reproduction in any medium or format, as long as you give appropriate credit to the original author(s) and the source, provide a link to the Creative Commons licence, and indicate if changes were made. The images or other third party material in this article are included in the article's Creative Commons licence, unless indicated otherwise in a credit line to the material. If material is not included in the article's Creative Commons licence and your intended use is not permitted by statutory regulation or exceeds the permitted use, you will need to obtain permission directly from the copyright holder. To view a copy of this licence, visit <http://creativecommons.org/licenses/by/4.0/>.

References

- [1] Malm J (2011) Inclusion of substances of very high concern in the candidate list. European Chemicals Agency (EACH), Helsinki
- [2] Morgan OM, Meinhardt DS (1999) Monopropellant selection criteria - hydrazine and other options. In: 35th AIAA/ASME/SAE/ASEE joint propulsion conference and exhibit 1999, AIAA paper no. 99–2595, Los Angeles, United States. doi: <https://doi.org/10.2514/6.1999-2595>
- [3] Ventura M, Mullens P (1999) The use of hydrogen peroxide for propulsion and power. In: 5th AIAA/ASME/SAE/ASEE joint propulsion conference and exhibit 1999, AIAA paper no. 99–2880, Los Angeles, USA. doi: <https://doi.org/10.2514/6.1999-2880>
- [4] Gohardani AS, Stanojev J, Demairé A, Anflo K, Persson M, Wingborg N, Nilsson C (2014) Green space propulsion: opportunities and prospects. *Prog Aerosp Sci* 71:128–149. <https://doi.org/10.1016/j.paerosci.2014.08.001>
- [5] Batonneau Y, Brahmi R, Cartoixa B, Farhat K, Kappenstein C, Keav S, Kharchafi-Farhat G, Pirault-Roy L, Saouabé M, Scharlemann C (2014) Green propulsion: catalysts for the European FP7 Project GRASP. *Top Catal* 57:656–667. <http://doi.org/10.1007/s11244-013-0223-y>
- [6] Amariei D, Rossignol S, Kappenstein C, Joulin JP (2006) Shape forming of Pt/Al₂O₃Si sol-gel catalysts for space applications. *Stud Surf Sci Catal* 162:969–976. [https://doi.org/10.1016/S0167-2991\(06\)81004-9](https://doi.org/10.1016/S0167-2991(06)81004-9)
- [7] S. Casu, B. Geiger, R. Kiemel, J.-Y. Lestrade, J. Anthoine (2019) Development and characterization of a catalyst for the decomposition of hydrogen peroxide. In: AIAA propulsion and energy forum 2019, AIAA paper no. 2019–4278, Indianapolis, United States. doi: <https://doi.org/10.2514/6.2019-4278>
- [8] Dolci S, Belli Dell'Amico D, Pasini A, Torre L, Pace G, Valentini D (2015) Platinum catalysts development for 98% hydrogen peroxide decomposition in pulsed monopropellant thrusters. *J Propul Power* 31:1204–1216. <https://doi.org/10.2514/1.B35590>
- [9] Gordon S, McBride BJ (1994) Computer program for calculation of complex chemical equilibrium compositions and applications. NASA, United States, Washington
- [10] Schumb WC, Satterfield CN, Wentworth RL (1955) Hydrogen peroxide. Reinhold Publishing Corporation, New York, 1955: 602–605
- [11] Meille V (2006) Review on methods to deposit catalysts on structured surfaces. *Appl Catal A: General* 315:1–17. <http://doi.org/10.1016/j.apcata.2006.08.031>
- [12] Brault P (2011) Plasma deposition of catalytic thin films: experiments, applications, molecular modelling. *Surf Coat Technol* 205:S15–S23. <https://doi.org/10.1016/j.apcata.2006.08.031>
- [13] Johnson RW, Hultqvist A, Bent SF (2014) A brief review of atomic layer deposition: from fundamentals to applications. *Mater Today* 17:236–246. <https://doi.org/10.1016/j.mattod.2014.04.026>
- [14] El Khakani MA, Chaker M, Le Drogoff B (1998) Iridium thin films deposited by radio-frequency magnetron sputtering. *J Vac Sci Technol A* 16:885–888. <https://doi.org/10.1116/1.581029>
- [15] Easton EB, Bonakdarpour A, Dahn JR (2006) Fe-CN oxygen reduction catalysts prepared by combinatorial sputter deposition. *Electrochem Solid-State Lett* 9:A463–A467. <https://doi.org/10.1149/1.2266157>
- [16] Kizling MB, Järås SG (1996) A review of the use of plasma techniques in catalyst preparation and catalytic reactions. *Appl Catal A: General* 147:1–21. [https://doi.org/10.1016/S0926-860X\(96\)00215-3](https://doi.org/10.1016/S0926-860X(96)00215-3)
- [17] Beni G, Schiavone LM, Shay JL, Dautremont-Smith WC, Schneider BS (1979) Electrocatalytic oxygen evolution on reactively sputtered electrochromic iridium oxide films. *Nature* 282:281–238. <https://doi.org/10.1038/282281a0>

- [18] Mukerjee S, Srinivasan S, Appleby AJ (1993) Effect of sputtered film of platinum on low platinum loading electrodes on electrode kinetics of oxygen reduction in proton exchange membrane fuel cells. *Electrochim Acta* 38:1661–1669. [https://doi.org/10.1016/0013-4686\(93\)85056-5](https://doi.org/10.1016/0013-4686(93)85056-5)
- [19] Atanasoski RT, Atanasoska LL, Cullen DA, Haugen GM, More KL, Vernstrom GD (2012) Fuel cells catalyst for start-up and shutdown conditions: electrochemical, XPS, and STEM evaluation of sputter-deposited Ru, Ir, and Ti on Pt-coated nanostructured thin film supports. *Electrocatalysis* 3:284–297. <https://doi.org/10.1007/s12678-012-0092-3>
- [20] Alvisia M, Galtieri G, Giorgi L, Giorgi R, Serra E, Signore MA (2005) Sputter deposition of Pt nanoclusters and thin films on PEM fuel cell electrodes. *Surf Coat Technol* 200:1325–1329. <https://doi.org/10.1016/j.surfcoat.2005.07.093>
- [21] Hirano S, Kim J, Srinivasan S (1997) High performance proton exchange membrane fuel cells with sputter-deposited Pt layer electrodes. *Electrochim Acta* 42:1587–1593. [https://doi.org/10.1016/S0013-4686\(96\)00320-9](https://doi.org/10.1016/S0013-4686(96)00320-9)
- [22] G. Ganske, G. Topalov, E. Slavcheva, W. Mokwa, U. Schnakenberg (2009) Sputtered platinum-iridium as catalyst for hydrogen fuel cells. *TRANSDUCERS 2009 International Solid-State Sensors, Actuators and Microsystems Conference, Denver, CO: 2106–2109*. doi: <https://doi.org/10.1109/SENSOR.2009.5285621>
- [23] Topalov G, Ganske G, Lefterova E, Schnakenberg U, Slavcheva E (2011) Preparation and properties of thin Pt–Ir films deposited by dc magnetron co-sputtering. *Int J Hydrogen Energy* 36:15437–15445. <https://doi.org/10.1016/j.ijhydene.2011.08.100>
- [24] Slavcheva E, Topalov G, Ganske G, Radev I, Lefterova E, Schnakenberg U (2010) Influence of sputtering pressure on surface structure and oxygen reduction reaction catalytic activity of thin platinum films. *Electrochim Acta* 55:8992–8997. <https://doi.org/10.1016/j.electacta.2010.08.047>
- [25] Slavcheva E, Radev I, Bliznakov S, Topalov G, Andreev P, Budevski E (2007) Sputtered iridium oxide films as electrocatalysts for water splitting via PEM electrolysis. *Electrochim Acta* 52:3889–3894. <https://doi.org/10.1016/j.electacta.2006.11.005>
- [26] Wessling B, van Ooyen A, Mokwa W, Schnakenberg U (2006) Iridium sputtered at varying pressures and target-substrate-distances evaluated for use as stimulation electrode material. In: *International conference of the IEEE engineering in medicine and biology society: 3353*. doi: <https://doi.org/10.1109/IEMBS.2006.260541>
- [27] Wessling B, Besmehn A, Mokwa W, Schnakenberg U (2007) Reactively sputtered iridium oxide: influence of plasma excitation and substrate temperature on morphology, composition, and electrochemical characteristics. *J Electrochem Soc* 154:83–89. <https://doi.org/10.1149/1.2713691>
- [28] Wessling B, Mokwa W, Schnakenberg U (2008) Sputtered Ir films evaluated for electrochemical performance I. Experimental results. *J Electrochem Soc* 155:61–65. <https://doi.org/10.1149/1.2844805>
- [29] Wessling B, Lüsebrink D, Mokwa W, Schnakenberg U (2008) Sputtered Ir films evaluated for electrochemical performance ii. Simulations *J Electrochem Soc* 155:66–74. <https://doi.org/10.1149/1.2844818>
- [30] Qing W, Liu F, Yao H, Sun S, Chen C, Zhang W (2020) Functional catalytic membrane development: a review of catalyst coating techniques. *Adv Coll Interface Sci* 282:102207. <https://doi.org/10.1016/j.cis.2020.102207>
- [31] Rogers DB (1972) Single crystals of transition-metal dioxides. *Inorganic Syntheses, Vol. 13* (Eds: F. A. Cotton), McGraw–Hill Book Company Inc. New York, US 1972:135–145. <https://doi.org/10.1002/9780470132449.ch27>
- [32] Lai SL, Guo JY, Petrova V, Rammath G, Allen LH (1996) Size-dependent melting properties of small tin particles: nanocalorimetric measurements. *Phys Rev Lett* 77:99–102. <https://doi.org/10.1103/PhysRevLett.77.99>
- [33] Buffat PH, Borrel JP (1976) Size effect on the melting temperature of gold particles. *Phys Rev A* 13:2287–2298. <https://doi.org/10.1103/PhysRevA.13.2287>
- [34] Büttner A, Probst A-C, Emmerich F, Damm C, Rellinghaus B, Döhring T, Stollenwerk M (2018) Influence of sputtering pressure on microstructure and layer properties of iridium thin films. *Thin Solid Films* 662:41–46. <https://doi.org/10.1016/j.tsf.2018.06.056>
- [35] J. A. Thornton (1988) Structure-Zone Models Of Thin Films. *Proc. SPIE 0821, Modeling of Optical Thin Films: 95–105*. doi: <https://doi.org/10.1117/12.941846>
- [36] Thornton JA (1986) The microstructure of sputter-deposited coatings. *J Vac Sci Technol A* 4:3059–3065. <https://doi.org/10.1116/1.573628>

Publisher's Note Springer Nature remains neutral with regard to jurisdictional claims in published maps and institutional affiliations.